# The Inspection of Raw- Silk Defects Using Image Vision

Qingtian Pan[1], Miao Chen[2], Baoqi Zuo[1], Yucai Hu[3]

[1]Soochow University, Suzhou City, Jiangsu CHINA

[2]Wuxi Entry-Exit Inspection Quarantine Bureau CHINA

[3]Yancheng Industry Career Technical College CHINA

Correspondence to:
Qingtian Pan email: 1149106160@qq.com

**ABSTRACT**

The inspection of defects is one of the most important aspects in the quality inspection of raw silk. We introduce a raw-silk defect detection system based on image vision and image analysis that is accurate and objective. In the experimental phase, we develop an image-acquisition section—which includes a charge-coupled device (CCD) image sensor, a telecentric lens, a light source, and a raw-silk winding device to capture the raw silk images steadily. After the image capture stage, an image-processing section tasked with threshold segmentation and morphology operations is carried out to obtain the defects of raw silk. To classify the raw-silk defects accurately and quickly, we propose an area method for the classification of raw-silk defects into five categories: larger defects, large defects, common defects, small defects, and smaller defects. Meanwhile, in order to recognize the common raw-silk defects—e.g., Bavella silk, nodes, and loose ends—that cannot be detected by the Uster evenness tester, the moment invariants of each segmented region of the images are extracted and used as the input of support vector machine(SVM).A SVM is designed as a classifier to recognize the samples. The experimental results show that the proposed method can recognize these common raw-silk defects effectively. According to the new classification and accurate recognition of raw-silk defects using the proposed method, we can improve the inspection standards for raw silk and advise raw-silk reeling enterprises seeking to optimize the technological parameters.

**Keywords:** image vision; raw-silk defects; defect classification; moment invariants; Support Vector Machine (SVM)

**INTRODUCTION**

Raw silk is an expensive natural fiber that has great affinity to human skin and is thus known as the “fiber queen.” Because raw silk is bonded together by cocoon filaments using multi-pass technology, there are many types of defects, such as cleanness defects—which produce protuberances and hairiness, decreasing the strength and stretch of the material—and neatness defects, which degrade the cohesion of the silk, causing breakage and cutting in the weaving process. Thus, the inspection of raw-silk defects is very important for raw-silk reeling and weaving enterprises.

Traditionally, raw silk is manually inspected for defects via seriplane inspection. Human inspection of raw silk has the following disadvantages. The visual inspection of similar and repetitive patterns can easily become boring. Human inspection has poor repeatability and constitutes a significant cost factor in the garment manufacturing process [1]. With the rapid development of modern electronic detection technology, the silk industry is eager to test electronic detection devices, which are objective and impartial and reduce the influence of human factors. From the 1990s to the beginning of the century, the Uster evenness tester, which detects the electrical-capacitance variation corresponding to the mass variation of a silk thread when it runs through a sensor split having a certain length, has been used to investigate the quality of raw silk. It has drawbacks, such as poor repeatability, a high manufacturing cost, and inaccurate measurement. It can only detect a minimum length of 8 mm. Thus far, electronic detection equipment only provides the coefficient of variation for evenness, the slubs number, the thick-place number, and the thin-place number of a certain length of raw silk, which are

not enough to evaluate the surface of the raw silk. Many other types of raw-silk defects—such as Bavella silk, nodes, and loose ends—cannot be identified by the Uster evenness tester.

Auto-inspection based on image vision and image-processing techniques is an interesting research subject. Yarn inspection has attracted considerable attention in recent years. Carvalho et al. proposed a system for measuring the hairiness of yarn using a coherent optical signal-processing technique, in steps of 1 mm [2]. Chen Ling et al. analyzed seriplane images of yarn using a digital image-processing instrument that performed smoothing treatment, thresholding segmentation, and image impairing [3]. Qin Weigang introduced a method for the on-line measurement of yarn evenness using a charge-coupled device (CCD) image sensor [4]. JI Jianzheng et al. used a video microscope to capture yarn images and then measured the linear density of the yarn via image processing [5]. However, few researchers have studied raw-silk defects, because there are many types of raw-silk defects, and the rating standard for these defects is very complicated.

The auto-inspection of raw silk based on image vision and image processing is the focus of future development. We propose a raw-silk defect detection and recognition system based on image vision and image analysis. The framework of the system is shown in *Figure 1*.

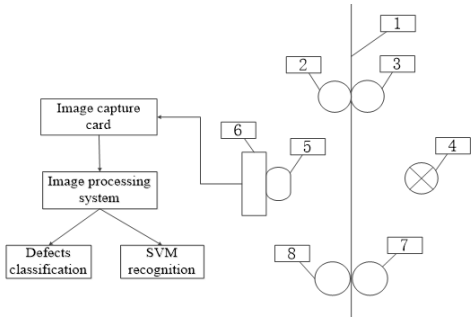


FIGURE 1. Schematic of the raw-silk defect detection and recognition system.

As is shown in *Figure 1*, the system components are (1) raw silk; (2, 3) tension clamps, which keep the raw silk moving stably; (4) a light source (OPT-LS82-W)—we adopt the back light illustration, with the light source placed on one side of the raw silk and the camera placed on the other side; (5) a telecentric lens, whose magnification is 6 and model type is MGTL60C; (6) a CCD line-scan camera (Dalsa S2-1y-05H40) with a resolution of 512, a pixel size of 14 μm × 14 μm, and a maximum line frequency of 65 kHz; and (7, 8) a raw-silk winding device, which drives the raw silk at a certain speed [6][7]. Images of the moving raw silk are captured and stored on a computer via an image capture card (Dalsa Xcelera-c1 LX1) that matches the CCD camera. Then, the images are processed by the image-processing system, and the thresholding segmentation and morphology operation are selected. Finally, the area method is implemented to classify the defects of the raw silk. The defects that cannot be detected by the Uster evenness tester—including Bavella silk, nodes, and loose-end defects—are recognized precisely by the support vector machine (SVM).

## CLASSIFICATION OF RAW-SILK DEFECTS

### Major Existing Classification Standard for Raw-Silk Defects

#### *Classification Standard for Raw-Silk Defects Based on Seriplane Inspection*

The seriplane inspection of raw silk involves a cleanness test and neatness test. At present, the test for raw silk references the national standard called the Testing Method for Raw Silk 2008, which is intended to provide the basis for the production and inspection of raw silk in China [8]. *Table I* and *Table II* and *Figure 2* present the defect classification standard and images of cleanness defects and neatness defects according to the Testing Method for Raw Silk (2008).

TABLE I. Classification standard for cleanness defects.

| Name of defect | | Defect description | Length/mm |
|---|---|---|---|
| Major defects (larger slubs) | | Length or diameter more than 10 times the minimum of the minor defects | 70 |
| Minor defects | Bavella Silk | Loose threads attached to silk strips | |
| | Large slubs | Swellings or shorter length but inflated parts of the silk | >7 |
| | Adhering husk | Cocoon silk part is folded and adhesion is tapered | |
| | Very long knots | Long knots or slightly shorter length and poor combined stitching of the knots | >10 |
| | Heavy corkscrew | Inflated corkscrews formed via one or more instances of cocoon silk twining the silk strip and whose diameters are larger than double that of the silk strip | Around 100 |
| Common defects | Small slugs | Inflated parts of the silk strip or the more inflated parts that are smaller than 2 mm | 2–7 |
| | Long knots | Knots whose ends are slightly long | 4–10 |
| | Corkscrew | Inflated corkscrews formed via one or more instances of cocoon silk twining the silk strip and whose diameters are smaller than double that of the silk strip | around 100 |
| | Ring | Ring of circles | >20 |
| | Loose ends | Division of the raw-silk trunk | >20 |

TABLE II. Classification standard for neatness defects.

| Type of defect | Defect description |
|---|---|
| Type 1 | (1) From Type 1 to Type 3, the number of defects increases. |
| | (2) Description of the defects for the three types: |
| Type 2 | a) Fine corkscrews are longer than 20 mm at the starting point. |
| | b) Loose end is longer than 10 mm at the starting point. |
| Type 3 | c) Length of the raw-silk nibs is <2 mm. |
| | d) Length of the knot end is <2 mm. |

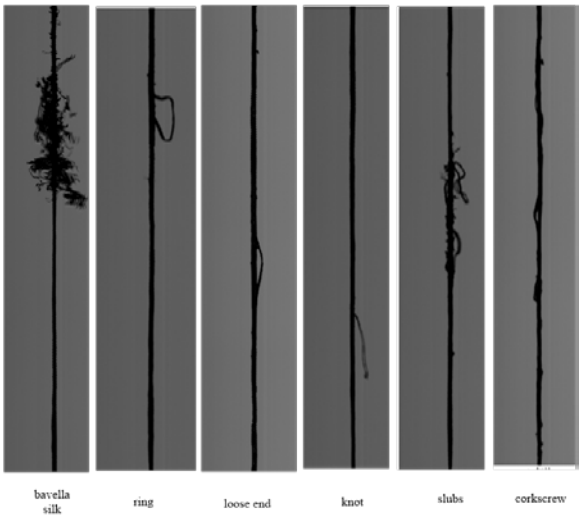


FIGURE 2. Images of raw-silk defects.

***Classification Standard for Raw-Silk Defects Based on Electronic Testing***

The International Raw Silk Association proposed an automatic detection standard for raw silk in 1995 [9]. It introduced thick and thin defects instead of cleanness defects of seriplane inspection, and the total number of thick and thin defects per 1,000 m was used for the classification. The index of uncleanness was introduced, replacing the neatness defects of seriplane inspection, and the total number of uncleannesses per 1,000 m was expressed. The types of raw-silk defects were defined by the International Raw Silk Association as follows: thick, with the mass of each 1 mm being >35%; thin, with the mass of each 1 mm being <40%; unclean, with the length being <4 mm and the mass of each 1 mm being >140%.

With the improvement of electronic detection technology, the International Standardization Organization established a new standard for the electronic detection of raw silk in 2014. This standard is mainly for the Uster tester method and optical testers that detect the photometric variation of the shadow of silk threads, which corresponds to the cross-sectional area variation of the thread. The raw-silk defects are divided into four categories: slubs, thick places, thin places, and small imperfection elements (SIE). Their definitions are as follows [10].

(1) Slubs

For the capacitive method, the length of the defect is no less than 1 mm, and the mass exceeds 80% of the average mass of the testing sample.

For the optical method, the length of the defect is no less than 1 mm, and the cross-sectional area exceeds 80% of the average cross-sectional area of the testing sample.

(2) Thick place

For the capacitive method, the length of the defect is no less than 10 mm, and the mass exceeds 35% to 80% of the average mass of the testing sample.

For the optical method, the length of the defect is equal to or greater than 10 mm, and the cross-sectional area exceeds 30% to 80% of the average cross-sectional area of the testing sample.

(3) Thin place

For the capacitive method, the length of the defect is no less than 10 mm, and the mass is more than 40% lower than the average mass of the testing sample.

For the optical method, the length of the defect is no less than 10 mm, and the cross-sectional area is more than 30% lower than the average cross-sectional area of the testing sample.

(4) SIE

The length of the defect is no greater than 1 mm, and the mass or cross-sectional area exceeds 80% of the average mass or the average cross-sectional area, respectively, of the testing sample.

**Classification Standard for Raw-Silk Defects Based on Image-Processing Method**

At present, seriplane inspection is the main inspection method for raw-silk defects in China. Seriplane inspection is too complex to clearly classify defects and perform rapid analysis. On the other hand, the capacitive method and optical method are too simple and inaccurate to reveal the full extent and characteristics of raw-silk defects. In this study, we first detect the defects of raw silk via thresholding segmentation and morphology operations. *Figure 3* and *Figure 4* show the contrast effects [8]. Then, referring to the classification standard for seriplane inspection, the area method—which is based on image vision—is employed to classify the raw-silk defects. According to the area method, the raw-silk defects are classified into the five categories of larger defects, large defects, common defects, small defects—which correspond to major defects, minor defects, common defects, and neatness defects of seriplane inspection, respectively—and smaller defects according to the minimum discrimination length of the human eye. As shown in *Table I* and *Table II*, the critical lengths of the major defects,

minor defects, common defects, and neatness defects are 70, 7, and 2 mm, respectively. The minimum discrimination length of the human eye is 0.1 mm; thus, defects shorter than 0.1 mm cannot be detected via seriplane inspection. The actual accuracy of our system reaches 2.5 μm; therefore, the system can detect defects shorter than 0.1 mm. These are a new type of defects called "smaller defects," which provide a better guarantee for the quality of the raw-silk appearance and a high loom speed. Next, according to the defect size of the raw-silk standard image, the width of all kinds of defects is defined. The widths of the larger defects, large defects, common defects, small defects, and smaller defects are 2, 1.5, 1.5, 1.2, and 1.2 times the average diameter, respectively. We consider the defects of the raw silk as a rectangle whose length and width is defined as previously mentioned. For the case of raw silk 20/22D, whose average diameter is 65 μm, the defect classification based on the image-processing method is presented in *Table III*.

FIGURE 3. Original image.

FIGURE 4. Image taken after the thresholding segmentation and morphology operations.

**RECOGNITION OF RAW-SILK DEFECTS BASED ON SVM**

*Figure 5* shows the process of recognition based on an SVM. Threshold segmentation is employed to separate the raw silk and background. The original features and attributes of the images are extracted via feature extraction to prepare for the SVM recognition, which is performed to train and recognize the raw-silk defects.

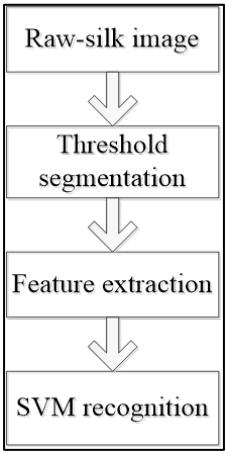


FIGURE 5. SVM processing flow chart.

**Threshold Segmentation**

Threshold segmentation subdivides a grayscale image into a binary image that consists of two regions: the object and the background. A threshold can be used to determine whether a pixel belongs to the object or the background. In this study, Otsu's method is used to perform automatic segmentation according to the different gray levels between the object and the background. Otsu's method takes an image, computes its histogram, and then determines the threshold value that maximizes the between-class variance $\sigma^2$.

*Figure 6* shows an original raw-silk image, and *Figure 7* shows the image after threshold segmentation via Otsu's method. The separation is obvious. We clearly observe the raw-silk defect. As shown in *Figure 7*, the raw silk is well-separated from the background.


FIGURE 6. Original raw-silk image.


FIGURE 7. Image taken after threshold segmentation.

TABLE III. Defect classification for raw silk 20/22D based on image-processing method.

| **Defects** | **Length/mm** | **Width/μm** | **Area/μm$^2$** |
|---|---|---|---|
| Larger defects | >70 | 2 × 65 | >9,100,000 |
| Large defects | 7–70 | 1.5 × 65 | 682,500–9,100,000 |
| Common defects | 2–7 | 1.5 × 65 | 195,000–682,500 |
| Small defects | 0.1–2 | 1.2 × 65 | 7,800–195,000 |
| Smaller defects | <0.1 | 1.2 × 65 | <7,800 |

## Feature Extraction

Image features are the original characteristics or attributes of an image. They are extracted for identification or classification with neural networks, and this process is called feature extraction. Feature extraction is essential because if the features do not have discrimination, the classifier performance is poor. To achieve a high recognition accuracy, we employ a widely used shape feature—moment invariants—to describe the regional features.

### *Moment Invariants*

The two-dimensional moment of order (p+q) of a digital image f(x, y) is defined as

$$m_{pq} = \int_{-\infty}^{+\infty}\int_{-\infty}^{+\infty} x^p y^q f(x,y)dxdy \qquad (1)$$

The center is defined as

$$M_{pq} = \int_{-\infty}^{+\infty}\int_{-\infty}^{+\infty} (x-\bar{x})^p (y-\bar{y})^q f(x,y)dxdy \qquad (2)$$

where

$$\bar{x} = \frac{m_{10}}{m_{00}} \quad \text{and} \quad \bar{y} = \frac{m_{01}}{m_{00}} \qquad (3)$$

The normalized central moment is defined as

$$\eta_{pq} = \frac{M_{pq}}{M_{00}^{\gamma}} \qquad \gamma = \frac{p+q}{2}+1 \qquad p+q=2, 3 \qquad (4)$$

Hu proposed seven moment invariants that could be derived from the second- and third-order central moments. The moment group had been proven to be invariant with rotation, translation, and size change [11, 12]. They are given as follows:

$$
\begin{aligned}
\phi_1 &= \eta_{20} + \eta_{02} \\
\phi_2 &= (\eta_{20} - \eta_{02})^2 + 4\eta_{11}^2 \\
\phi_3 &= (\eta_{30} - 3\eta_{12})^2 + (3\eta_{21} - \eta_{03})^2 \\
\phi_4 &= (\eta_{30} + \eta_{12})^2 + (\eta_{21} + \eta_{03})^2 \\
\phi_5 &= (\eta_{30} - 3\eta_{12})(\eta_{30} + \eta_{12})[(\eta_{30} + \eta_{12})^2 - 3(\eta_{21} + \eta_{03})^2] + \\
&\quad (3\eta_{21} - \eta_{03})(\eta_{21} + \eta_{03})[3(\eta_{30} + \eta_{12})^2 - (\eta_{21} + \eta_{03})^2] \\
\phi_6 &= (\eta_{20} - \eta_{02})[(\eta_{30} + \eta_{12})^2 - (\eta_{21} + \eta_{03})^2] \\
&\quad + 4\eta_{11}(\eta_{30} + \eta_{12})(\eta_{21} + \eta_{03}) \\
\phi_7 &= (3\eta_{21} - \eta_{03})(\eta_{30} + \eta_{12})[(\eta_{30} + \eta_{12})^2 - 3(\eta_{21} + \eta_{03})^2] + \\
&\quad (3\eta_{12} - \eta_{30})(\eta_{21} + \eta_{03})[3(\eta_{30} + \eta_{12})^2 - (\eta_{21} + \eta_{03})^2]
\end{aligned}
\tag{5}
$$

We use the absolute value of the *log* instead of the moment-invariant values. Use of the *log* can reduce the dynamic range. The absolute value avoids the complex numbers that result in computing the *log* of negative moment invariants. The shapes of three kinds of raw-silk defects are different, which make the seven moment invariants differ. After the extraction of the shape features using the moment invariants, the SVM is employed for recognition.

## Recognition with SVM

### *SVM for Classification*

The SVM is a data-learning method based on the theory of statistical learning [13]. Compared to artificial neural networks, the SVM can easily overfit training samples and has better generalization ability for test samples [14][15]. One of the main reasons for the wide application of the SVM is its capacity to handle nonlinearly separable data. The SVM involves searching for a hyperplane that satisfies the requirement of classification, which is the best support vector to distinguish two different classes, under the condition of limited information based on a small amount of samples [16][17].

The recognition of raw-silk defects is a nonlinear classification model. For non-linearly separable data, a nonlinear mapping function—$\phi$: RN→RD, $\chi \rightarrow \phi(\chi)$—is used to map them into a higher-dimension feature space where the hyperplane classifier can be applied. The nonlinear mapping function is called the kernel function [18]. Using the kernel function, the nonlinear SVM is given as

$$
\mathrm{h}(x) = \mathrm{sgn}\left(\sum_{i \in SV} \alpha_i \, y_i k(x_i, x) + b\right), \tag{6}
$$

where $x_i \in \mathrm{R}^N$ is the support vector learned by the SVM, and $k(x_i,x)$ is the kernel function. Commonly used kernel functions include linear functions, polynomial functions, radial basis functions (RBFs), and Sigmoid functions [13][19]. RBF kernels typically perform better for pattern classification [20],hence we use the RBF kernel function in this study.

The SVM is a two-category classification. We generalize the SVM classification and build a multiclass classification by combining different two-category classifiers. It includes two main methods: one against all and one against one. One against all sets one as a class and the other as another class. Then, if there are n classes, n classifiers of the SVM are generated. One against one selects two different classes as one SVM classifier. Then, it generates n(n-1)/2 SVM classifiers [19]. Raw-silk defect recognition is a multiclass classification problem. One against one with voting is employed in this study. That is, if the SVM classifier of the training set (A, B) determines x to be of class A, A receives one vote. x belongs to the class that receives the most votes.

### *Experimental Results*

There are four types of raw-silk images: Bavella silk, nodes, loose end, and normal silk. The number of each type is 80. We extract the normalized seven feature parameters of the moment invariants from the four types of raw-silk images as the input vector, and three groups of experiments with different numbers of training samples and test samples are selected. We use the RBF kernel function and adopt the one against one with voting method to classify unknown samples. The experimental results are shown in *Table IV.*

*Table IV* shows that the proposed method can recognize different types of raw-silk defects effectively. The identification accuracy for the normal silk, Bavella silk, and nodes is 100%. With the increase of the number of training samples, the identification accuracy for the loose ends improves, and the maximum value is 93.3% (when a loose end is short, it is probably mistaken for a node). The maximum average identification accuracy of the raw-silk defects is 98.4%, which is very high.

TABLE IV. Identification results.

| Groups | Training samples | Test samples | Defects | Original number | Identification number | Recognition accuracy (%) | Average recognition accuracy (%) |
|---|---|---|---|---|---|---|---|
| 1 | 120 | 200 | No defects | 50 | 50 | 100 | 96 |
| | | | Bavella silk | 50 | 50 | 100 | |
| | | | nodes | 50 | 58 (8 loose ends) | 100 | |
| | | | loose end | 50 | 42 | 84 | |
| 2 | 160 | 160 | No defects | 40 | 40 | 100 | 97.5 |
| | | | Bavella silk | 40 | 40 | 100 | |
| | | | nodes | 40 | 44 (4 loose ends) | 100 | |
| | | | loose end | 40 | 36 | 90 | |
| 3 | 200 | 120 | No defects | 30 | 30 | 100 | 98.4 |
| | | | Bavella silk | 30 | 30 | 100 | |
| | | | nodes | 30 | 32 (2 loose ends) | 100 | |
| | | | loose end | 30 | 28 | 93.3 | |

## CONCLUSION

A new system for the detection and recognition of defects in raw silk based on image vision and image analysis is proposed. Compared to seriplane inspection and the Uster evenness test, the new system, which is composed of an image-acquisition section and an image-processing section, is more accurate and objective. First, raw-silk images are captured and processed by the image-acquisition and image-processing systems. Then, an area method is used for the classification of the raw-silk defects into five categories: larger defects, large defects, common defects, small defects, and smaller defects. Finally, the moment invariants of the selected images are extracted, and the SVM is employed to recognize the common raw-silk defects, which are Bavella silk, nodes, and loose ends. The experimental results show that the SVM recognition is effective and accurate. The maximum average identification accuracy is 98.4 percent.

In future studies, we aim to establish an evaluation standard for the appearance of raw silk based on the new classification of raw-silk defects. We will also study the relationship between the silk-reeling technique and the raw-silk defects. According to the defect information obtained using the SVM, we can provide information to raw-silk reeling enterprises and prompt them to change their production technology for improving the appearance of raw silk.


## ACKNOWLEDGEMENT

The authors are grateful for the support of the Second Phase of Jiangsu Universities' Distinctive Discipline Development Program for Textile Science and Engineering of Soochow University, the Natural Science Foundation of China (Nos. 51303117 and 61473201), the Graduate Student Innovation Project of Jiangsu Province (KYZZ15-0327), and the Wuxi Entry-Exit Inspection Quarantine Bureau.


## REFERENCES


[1] Nateri, A. S., Ebrahimi, F and Sadeghzade, N, "Evaluation of yarn defects by image processing technique", Optik -International Journal for Light and Electron Optics, 2014, Vol. 125, No.125, pp.5998-6002.

[2] Carvalho, V. H et al., "Optical yarn hairiness measurement system", IEEE International Conference on IndustrialInformatics, 2007, Vol. 1, pp. 359-364.

[3] Cheng, L et al., "Digital image processing of cotton yarn seriplane", Computer and Information Application (ICCIA), 2010, Vol.1, pp. 274-277.

[4] Qin ,W.G., "On-line yarn evenness detection using CCD image sensor". 2011 Chinese Control and Decision Conference (CCDC), 2011, pp.1787- 1790.

[5] Zheng,J,J et al., “Measurement of yarn linear density based on digital image processing”, Journal of Textile Research , 2011, Vol.32, No.10, pp.42-46.
[6] Li, J.J et al., “A Direct Measurement Method of Yarn Evenness Based on Machine Vision”, Journal of Engineered Fabrics & Fibers, 2015,Vol.10, No.4, 95-102.
[7] Wang, C et al., “The obtainment and recognition of raw silk defects based on machine vision and image analysis”, Journal of the Textile Institute , 2015, Vol.107, No.3, pp.316-326.
[8] GB/T 1798-2008.Testing method for raw silk,China,2008.
[9] Sericulture and Silk Production:A Handbook, International Raw Silk Association, 1995.
[10] ISO 15625. Silk — Electronic test method for defects and evenness of raw silk, 2014.
[11] Hu, M.K., “Visual pattern recognition by moment invariants”, IIRE Transactions on Information Theory, 1962, Vol.8, No.2, pp.179-187.
[12] Yang K et al., “Shape-based foreign body recognition of train roof using invariant moments”, Optik; 2013, Vol.124, pp.5181-5183.
[13] Nelson, J. D et al., “Signal theory for SVM kernel design with applications to parameter estimation and sequence kernels” , Neurocomputing, 2008, Vol.72, pp.15-22.
[14] Vapnik, V. N. “Statistical Learning Theory. Encyclopedia of the Sciences of Learning”, Statistical Learning Theory. Encyclopedia of the Sciences of Learning, 2010, Vol.41,No .4, pp.3185-3185.
[15] Tong, S., Koller, D., “Support vector machine active learning with applications to text classification”, Journal of Machine Learning Research ,2001, Vol.2 ,No.1, pp.45-66.
[16] Cortes, C., Vapnik, V., “Support-Vector Networks. Machine Learning”, Machine Leaming, 1995, Vol.20 , No.3, pp.273-297.
[17] Osuna, E., Freund, R and Girosi, F, “An Improved Training Algorithm for Support Vector Machines”, Neural Networks for Signal Processing, 1998,pp. 24-26.
[18] Shen, L. L. and Ji, Z., “Gabor Wavelet Selection and SVM Classification for Object Recognition”, Acta Automatica Sinica, 2009, Vol.35, No.4, pp.350-355.
[19] Luo, Y., Wu, C. M and Zhang, Y, “Facial expression recognition based on fusion feature of PCA and LBP with SVM”, Optik,2013, Vol.124, No.17, pp.2767-2770.
[20] Abe,D., “Support Vector Machines for Pattern Classification, 2nd ed., SpringerVerlag, London ”, UK, 2010.

**AUTHORS’ ADDRESSES**

**Qingtian Pan**
**Baoqi Zuo**
Soochow University
199 Renai Road
Suzhou City
Suzhou, Jiangsu 215123
CHINA

**Miao Chen**
Wuxi Entry-Exit Inspection Quarantine Bureau
CHINA

**Yucai Hu**
Yancheng Industry Career Technical College
CHINA